

On 2D Periodic Hexagonal Cells

*R. Delbourgo*¹

School of Mathematics and Physics, University of Tasmania
GPO Private Bag 37, Hobart, Australia 7001

Abstract

Graphene, the new wondrous material, is a perfect example of a two-dimensional hexagonal crystal unlike any other. Here we exhibit some of the characteristic directional features associated with hexagonal cells, emphasising the sixfold symmetry. We depict the X-ray, vibrational and electronic band structures to be expected in such systems via 2 dimensional contour plots.

¹electronic address: bob.delbourgo@utas.edu.au

1 Introduction

It is little wonder that graphene has captured the interest of physicists or materials scientists and no surprise that it is the centrepiece of the 2010 Nobel Physics Prize. The reason for the great excitement lies in its remarkable transport properties and amazing strength plus the fact that technology has advanced to the stage where graphene can be produced in relatively large sheets, on a variety of substrates. A very bright future is predicted for it. Thus it possesses very low resistivity, high opacity and can furnish the photonics, spintronics and electronic industry with a low cost alternative to silicon.

There are numerous review articles [1, 2, 3, 4, 5] on this subject and a veritable avalanche of research papers has appeared, describing or exploring different properties. These concern its electronic characteristics, its vibrational properties, its edge effects, the Dirac-like properties of quasiparticles at the corners of Brillouin zones [6, 7, 8, 9], anomalous Hall effects, etc. Our aim in this paper is very modest: we wish to illustrate its beautiful directional properties in a manner that might benefit teachers of condensed matter physics: the 2D hexagonal symmetry is somewhat unfamiliar and can serve as a nice extension of the standard square symmetry analysis [10].

The paper is set out as follows. Section 2 contains the basic notation and its consequences for glancing X-rays. In Section 3 we discuss the oscillation modes within a hexagon, clamped at its edges. These represent the energy levels of a particle held in the infinite hexagonal well; the results are no doubt familiar to the graphene experts but are probably not widely known to the usual quantum mechanics practitioners, who often resort to rectangular boundary conditions. We also consider the modes corresponding to antinodes at the edges because these are subsequently needed for discussing the Kronig-Penney model in Section 5. Section 4 is devoted to idealised vibrational modes (longitudinal and transverse) of the atoms themselves, assuming nearest neighbour interactions. Here, as in Section 3, our aim is to illustrate the hexagonal symmetry of the motions. In the last Section we describe the electronic band structure, using the approximation of delta-function walls between adjoining cells rather than the tight-binding approximation used in most expositions. In order to keep the analysis simple, nowhere do we study edge effects (armchair, zigzag, corrugations [11]) or multilayer graphene; for such elaboration we refer the reader to research reviews. We hope that this paper will serve as a useful extension of the usual quantum mechanical prob-

lems encountered by college students and highlight the beautiful hexagonal symmetry of the principal properties of graphene.

2 Bases and X-Ray Features

Let us set down our notation which will be used in subsequent sections. The basic hexagonal cell (with side length ℓ) is drawn in Figure 1 and our coordinate system is centred there. The fundamental cell vectors are

$$\mathbf{a} = (3, -\sqrt{3})\ell/2, \quad \mathbf{b} = (3, \sqrt{3})\ell/2. \quad (1)$$

Any two nearby corner points such as carbon atoms at U and V can be taken as centres of X-ray scattering so that all lattice points are generated by translation:

$$\begin{aligned} \mathbf{u}_{rs} &= \mathbf{u}_{00} + r\mathbf{a} + s\mathbf{b} = (3r + 3s - 1, \sqrt{3}(s - r - 1))\ell/2 \\ \mathbf{v}_{rs} &= \mathbf{v}_{00} + r\mathbf{a} + s\mathbf{b} = (3r + 3s + 1, \sqrt{3}(s - r - 1))\ell/2, \end{aligned} \quad (2)$$

where r and s are integers. The basic reciprocal lattice, drawn in Figure 2, is nothing more than a scaled version of the original lattice, rotated by 30° with side length $4\pi/3\sqrt{3}\ell$. Its fundamental vectors are

$$\mathbf{A} = (1, -\sqrt{3})2\pi/3\ell, \quad \mathbf{B} = (1, \sqrt{3})2\pi/3\ell. \quad (3)$$

Then, according to the Von Laue conditions for constructive interference, whenever the change of wave number is (R and S are integers)

$$\Delta\mathbf{k} = R\mathbf{A} + S\mathbf{B} = (R + S, (S - R)\sqrt{3})2\pi/3\ell, \quad (4)$$

X-rays directed *along* the graphene plane will of course be diffracted by the lattice. However because there are *two* atoms decorating each unit cell there is a modulating factor $1 + \exp[(R + S)2\pi/3] \propto 2 \cos[\pi(R + S)/3]$ apart from an irrelevant phase; this means that diffraction will be greatest when $R + S$ is exactly divisible by 3 but that there are no missing orders of diffraction.

3 The hexagonal well

The literature on the equilateral triangular drum is old indeed; it goes back to Lamé [12] and Pockels [13]. A very nice series of reviews on this topic has been

written by McCartin [14], discussing the completeness, orthogonality and multiplicity of the solutions, subject to Dirichlet and Neumann conditions at the edge of the triangle. It is not hard to adapt the solutions to the case of the hexagon and we shall do so shortly. (As a matter of fact the solutions of the equilateral triangle are embedded in a one-sixth section of the hexagon.) Here is an outline of the main steps.

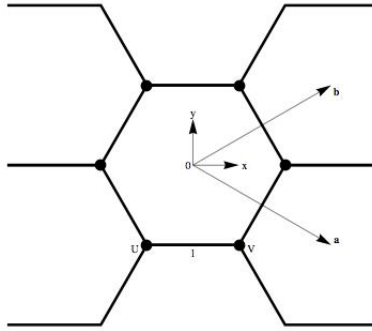


Figure 1: Basic cell vectors. Any two adjoining C atoms such as U and V can be taken as the basic cell components.

First of all introduce triangular coordinates, u, v, w centred at the origin with $u + v + w = 0$, as illustrated in Figure 3. The maximum values of these coordinates within the hexagon is the radius of the incircle $r = \ell\sqrt{3}/2$ and we see that in terms of the normal Cartesian coordinates,

$$u = -y, \quad v - w = \sqrt{3}x. \quad (5)$$

The second step is to note that the Schrödinger or Helmholtz equation for a free particle of energy E in the cell, namely

$$\left[\frac{\partial^2}{\partial x^2} + \frac{\partial^2}{\partial y^2} + k^2 \right] \psi(x, y) = 0; \quad k^2 = \frac{2ME}{\hbar^2},$$

may be transcribed into triangular coordinates:

$$\left[\frac{\partial^2}{\partial u^2} + 3 \frac{\partial^2}{\partial (v-w)^2} + k^2 \right] \psi(x, y) = 0, \quad (6)$$

cleverly allowing for cyclic sums of separable solutions of the form,

$$\psi(u, v, w) = [\cos(k_1 u) + C \sin(k_1 u)] \left[\cos(k_2 - k_3) \frac{(v-w)}{3} + D \sin(k_2 - k_3) \frac{(v-w)}{3} \right]$$

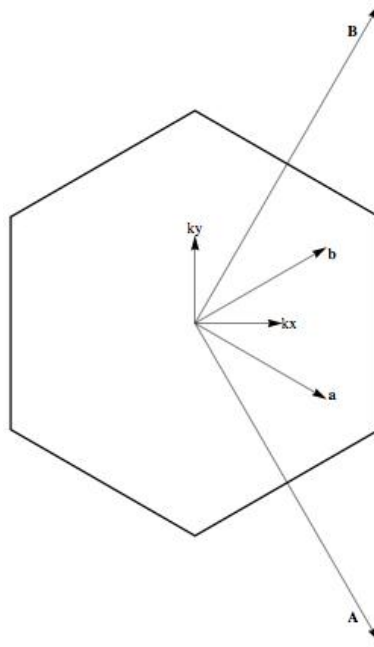


Figure 2: Brillouin zone and its basis vectors **A** and **B**.

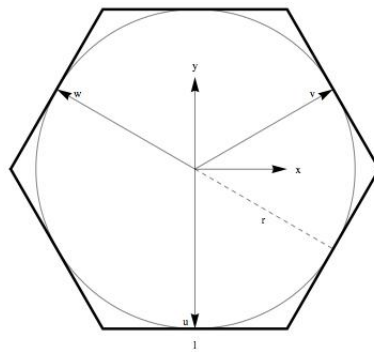


Figure 3: Triangular coordinates for describing modes of oscillation.

$$\begin{aligned}
& + [\cos(k_2u) + C \sin(k_2u)] [\cos(k_3 - k_1) \frac{(v-w)}{3} + D \sin(k_3 - k_1) \frac{(v-w)}{3}] \\
& + [\cos(k_3u) + C \sin(k_3u)] [\cos(k_1 - k_2) \frac{(v-w)}{3} + D \sin(k_1 - k_2) \frac{(v-w)}{3}] \quad (7)
\end{aligned}$$

where $k_1 + k_2 + k_3 = 0$ and $k^2 = 2(k_1^2 + k_2^2 + k_3^2)/3 = 4(k_1^2 + k_2^2 + k_1k_2)/3$. The third step is to pick out symmetric or antisymmetric solutions under reflection about a vertical diagonal; this selects out sin or cos functions in fact. Typically one finds [14] the (Dirichlet) quantized solutions $k_i = \pi n_i/r = 2\pi n_i/\sqrt{3}\ell$ – the case of interest for this section:

$$\begin{aligned}
\psi_{D \text{ sym/anti}} &= \sin \frac{\pi n_1 u}{r} \cdot \cos / \sin \frac{\pi(n_2 - n_3)(v-w)}{3r} + \\
&\sin \frac{\pi n_2 u}{r} \cdot \cos / \sin \frac{\pi(n_3 - n_1)(v-w)}{3r} + \\
&\sin \frac{\pi n_3 u}{r} \cdot \cos / \sin \frac{\pi(n_1 - n_2)(v-w)}{3r}, \quad (8)
\end{aligned}$$

where n_i are non-zero integers subject to $n_1 + n_2 + n_3 = 0$. It suffices to take $n_1 \geq n_2 > 0$ to obtain distinct modes (in the antisymmetric configuration n_1 and n_2 need to be different for a nonvanishing answer). Hence the quantized energy levels are given by

$$k_{n_1, n_2, n_3}^2 = 8\pi^2(n_1^2 + n_2^2 + n_3^2)/9\ell^2 = 16\pi^2(n_1^2 + n_2^2 + n_1n_2)/9\ell^2. \quad (9)$$

While we are discussing this topic let us note [14] the Neumann solutions (effectively antinodes along the hexagon edges) as we will require them later:

$$\begin{aligned}
\psi_{N \text{ sym/anti}} &= \cos \frac{\pi n_1 u}{r} \cdot \cos / \sin \frac{\pi(n_2 - n_3)(v-w)}{3r} + \\
&\cos \frac{\pi n_2 u}{r} \cdot \cos / \sin \frac{\pi(n_3 - n_1)(v-w)}{3r} + \\
&\cos \frac{\pi n_3 u}{r} \cdot \cos / \sin \frac{\pi(n_1 - n_2)(v-w)}{3r}. \quad (10)
\end{aligned}$$

We have illustrated some of the lowest few modes in Figures 4 to 6 in the form of contour plots rather than 3D plots as they are easier to comprehend (the lightest shaded areas are the maxima while the darkest correspond to minima). They show the lovely hexagonal features expected of the vibrations. The fundamental Neumann mode is depicted in Figure 7 even though it is not

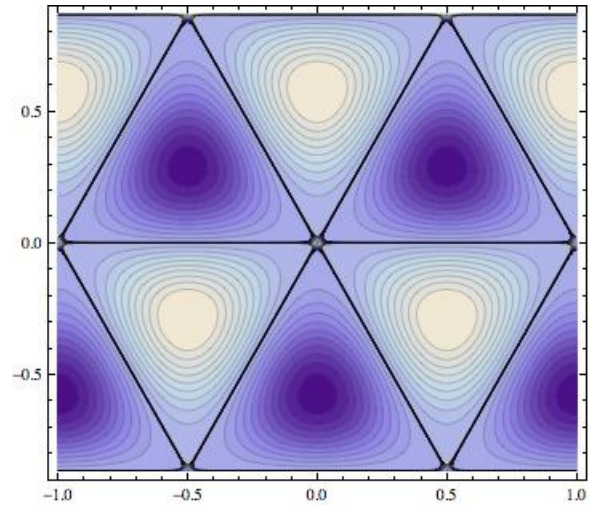


Figure 4: Fundamental mode (1,1) of the unit hexagonal well.

required for the present purposes. [It should be noted that triangular cuts within the hexagon describe the modes for an equilateral triangle.] McCartin has analysed the orthogonality and completeness properties of solutions (8) and (10) so we refer the reader to his review article.

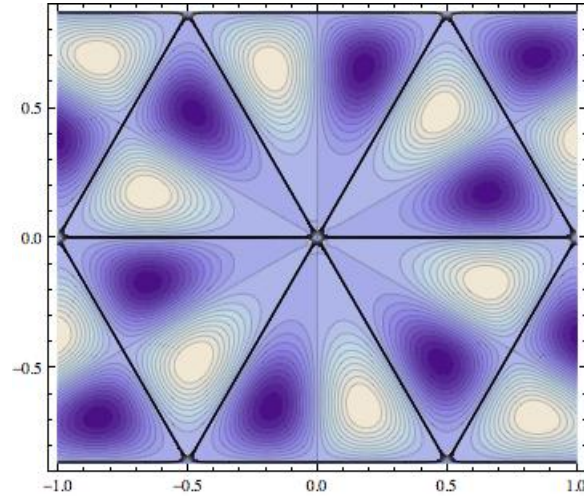


Figure 5: Antisymmetrical overtone (2,1) of the unit hexagonal well.

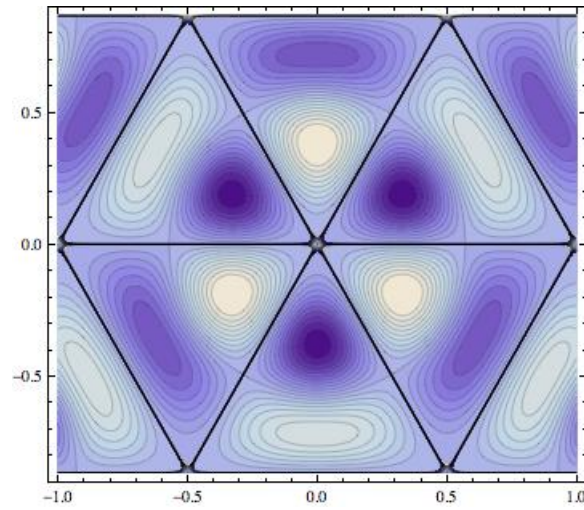


Figure 6: Symmetrical overtone (2,1) of the unit hexagonal well.

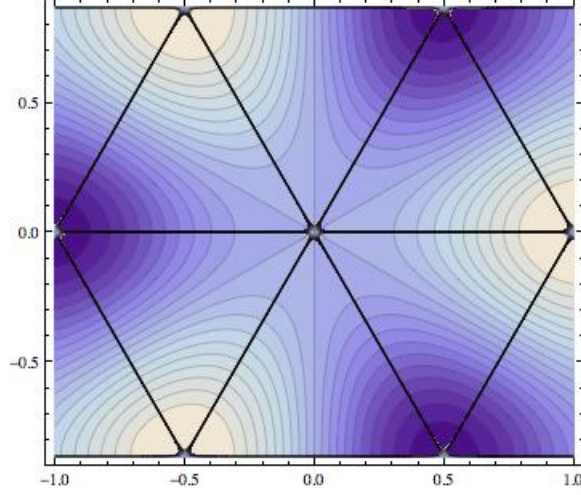


Figure 7: Basic Neumann mode (1,0) of the unit hexagonal well.

4 Vibrational Features

Let us begin by tackling vertical (out of plane) transverse oscillations. Regarding the graphene sheet as some sort of trampoline under fixed tension and considering only nearest neighbour interactions, the downward acceleration on a C atom located at \mathbf{u}_{rs} is determined by the adjoining vertical displacements relative to the atoms at $\mathbf{v}_{rs}, \mathbf{v}_{rs-1}, \mathbf{v}_{r-1s}$. Hence vibrations are described by the simple harmonic equation,

$$d^2U_{rs}/dt^2 = -\Omega^2(3U_{rs} - V_{rs} - V_{rs-1} - V_{r-1s}), \quad (11)$$

where Ω is a characteristic frequency associated with the “tension” of the links and how strongly or loosely the C atoms adhere to the substrate. Similarly for the twin atom located at \mathbf{v}_{rs} one obtains

$$d^2V_{rs}/dt^2 = -\Omega^2(3V_{rs} - U_{rs} - U_{rs+1} - U_{r+1s}). \quad (12)$$

Looking for plane wave solutions [$\mathbf{k} = (k_x, k_y)$ below], at the positions summarized by (2),

$$U_{rs} = U \exp[i(\mathbf{k} \cdot \mathbf{u}_{rs}) - \omega t], \quad V_{rs} = V \exp[i(\mathbf{k} \cdot \mathbf{v}_{rs}) - \omega t]$$

one arrives at two coupled equations for the amplitudes of the cell atoms at U and V:

$$\omega^2 U = \Omega^2[3U - Ve^{ik_x \ell} - 2Ve^{-ik_x \ell/2} \cos(k_y \ell \sqrt{3}/2)]$$

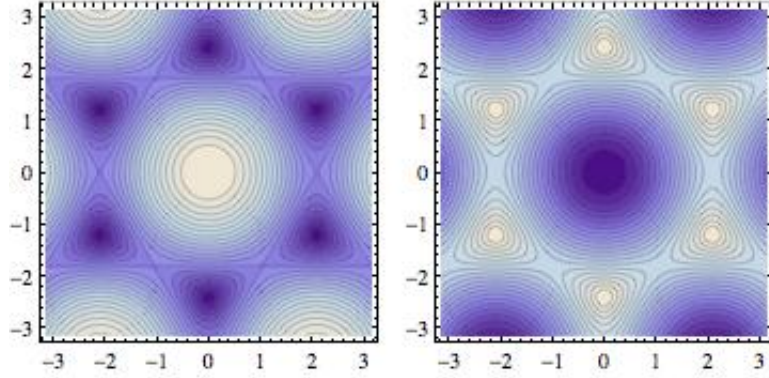


Figure 8: $\omega - k$ dispersion relation for acoustic and optical transverse modes (scaled by Ω) within the fundamental Brillouin zone.

$$\omega^2 V = \Omega^2 [3V - Ue^{-ik_x \ell} - 2Ue^{ik_x \ell/2} \cos(k_y \ell \sqrt{3}/2)], \quad (13)$$

producing the eigenvalue equation

$$(\omega^2/3\Omega^2 - 1)^2 = (1 + 4c_y^2 + 4c_x c_y)/9; \quad c_x \equiv \cos(3k_x \ell/2), c_y \equiv \cos(\sqrt{3}k_y \ell/2)$$

or dispersion relation between frequency and wavenumber for transverse vertical acoustic (-) and optical (+) modes:

$$\omega_{\pm} = \Omega [3 \pm \sqrt{1 + 4c_x c_y + 4c_y^2}]. \quad (14)$$

This dispersion relation for the two modes is shown in Figure 8. In the long wavelength limit,

$$\omega_-^2/\Omega^2 \simeq 3\ell^2(k_x^2 + k_y^2)/4, \quad \text{so} \quad v_{acoustic} = 2\Omega/\sqrt{3}\ell, \quad (15)$$

whereas $\omega_+ \simeq \sqrt{6}\Omega$ for optical vibrations. The acoustic and optical modes remain separated when the wave vector \mathbf{k} is directed along x even at the edge of the Brillouin zone, but they merge when \mathbf{k} is directed along y and a corner (a so-called Dirac point) of the zone is approached. It is the instabilities in the vertical motion that apparently tend to make graphene sheets ripple or even curl up into tubes.

Next we shall study the oscillations of the C atoms within the graphene plane. This time we are dealing with two-dimensional vector displacements

$\mathbf{U} = (U_x, U_y)$, $\mathbf{V} = (V_x, V_y)$ for the atoms located at positions determined by (2), rather than the vertical displacements considered previously. For small vibrations we assume that the restoring force is proportional to the extension in the direction of the link; so if one defines three unit vectors $\mathbf{e}_{1,2,3}$ along each of the links, the total restoring force of the atom at \mathbf{U} summed over the three links is

$$[(\mathbf{V}_{rs} - \mathbf{U}_{rs}) \cdot \mathbf{e}_1] \mathbf{e}_1 + [(\mathbf{V}_{r-1s} - \mathbf{U}_{rs}) \cdot \mathbf{e}_2] \mathbf{e}_2 + [(\mathbf{V}_{rs-1} - \mathbf{U}_{rs}) \cdot \mathbf{e}_3] \mathbf{e}_3$$

apart from an overall factor. Resolving the \mathbf{e}_i into Cartesian components, we get the equation pair for the \mathbf{U} atom (ϖ is the horizontal characteristic frequency),

$$\ddot{U}_{xrs}/\varpi^2 = -3U_{xrs}/2 + V_{xrs} + (V_{xr-1s} + V_{xrs-1})/4 + \sqrt{3}(V_{yrs-1} - V_{yr-1s})/4 \quad (16)$$

$$\ddot{U}_{yrs}/\varpi^2 = -3U_{yrs}/2 + 3(V_{yr-1s} + V_{yrs-1})/4 + \sqrt{3}(V_{xrs-1} - V_{xr-1s})/4. \quad (17)$$

A similar equation applies to the vector displacement \mathbf{V} of the \mathbf{V} atom alongside:

$$\ddot{V}_{xrs}/\varpi^2 = -3V_{xrs}/2 + U_{xrs} + (U_{xr+1s} + U_{xrs+1})/4 + \sqrt{3}(U_{yrs+1} - U_{yr+1s}) \quad (18)$$

$$\ddot{V}_{yrs}/\varpi^2 = -3V_{yrs}/2 + 3(V_{yr+1s} + V_{yrs+1})/4 + \sqrt{3}(U_{xrs+1} - U_{xr+1s})/4. \quad (19)$$

For vibrations of circular frequency ω and wave number \mathbf{k} , one arrives at the secular equation,

$$\begin{pmatrix} W & 0 & 1 + c_y e^{-i\chi}/2 & -i\sqrt{3}s_y e^{-i\chi}/2 \\ 0 & W & -i\sqrt{3}s_y e^{-i\chi} & 3c_y e^{-i\chi}/2 \\ 1 + c_y e^{i\chi}/2 & i\sqrt{3}s_y e^{i\chi}/2 & W & 0 \\ i\sqrt{3}s_y e^{i\chi}/2 & 3c_y e^{i\chi}/2 & 0 & W \end{pmatrix} \begin{pmatrix} U_x \\ U_y \\ V_x e^{ik_x \ell} \\ V_y e^{ik_x \ell} \end{pmatrix} = 0, \quad (20)$$

where $W \equiv \omega^2/4\varpi^2 - 3/2$, $\chi \equiv 3k_x \ell/2$, $c_y \equiv \cos(\sqrt{3}k_y \ell/2)$, $s_y \equiv \sin(\sqrt{3}k_y \ell/2)$ and ϖ stands for a characteristic frequency of planar oscillations, which is not necessarily equal to the value Ω for vertical oscillations because of the the substrate's influence.

This leads to the set of roots (dispersion relations):

$$\omega/\varpi = 0, \quad 2\sqrt{3}, \quad (3 - \sqrt{1 + 4c_x c_y + 4c_y^2}), \quad (3 + \sqrt{1 + 4c_x c_y + 4c_y^2}). \quad (21)$$

The first two roots may be ignored (the first is static displacement and the second is dispersionless). However, the third and fourth planar roots are strikingly similar to the vertical motion roots (14) (acoustic and optical), except that the oscillation frequency is not necessarily the same.

5 Kronig-Penney electron band model

We now turn to a model of the electronic energy bands which is a generalization of the one-dimensional Kronig-Penney scheme – instead of the tight-binding approximation which is more popular. To that end, we envisage a series of δ -function potential walls lying along the carbon links as that is where the electron clouds are at their most prominent. Any stray negative charge carrier would encounter these repulsive barriers, except of course at the cell corners where they would feel the attraction from the C nuclei. Therefore as our model we may envisage loose electrons as moving freely within the cells until they hit a cell edge, where the wave function discontinuity across the cell boundary is proportional to the wave function there (which is itself continuous). This should mimic the periodic properties and symmetry features of more realistic models.

Consider then the following parametrizations of the symmetric wave function Ψ_0 for the cell round the origin, drawn in Figure 1, and the wave function Ψ_1 for the cell below it (centred at $x = 0$, $y = -\sqrt{3}\ell$). One must allow for both Dirichlet *and* Neumann boundary conditions – the analogues of $\sin(kx)$ and $\cos(kx)$ that are included in the one-dimensional analysis. Here we do not consider antisymmetric solutions, since the model merely serves as an example to illustrate the hexagonal features of the bands – the true nature of the bands can in fact only be revealed through experiments.

$$\begin{aligned} \Psi_j = & [A_j \sin(k_1 u) + B_j \cos(k_1 u)] \cdot \cos(k_1 + 2k_2)(v - w)/3 + \\ & [A_j \sin(k_2 u) + B_j \cos(k_2 u)] \cdot \cos(2k_1 + k_2)(v - w)/3 - \\ & [A_j \sin((k_1 + k_2)u) - B_j \cos((k_1 + k_2)u)] \cdot \cos(k_1 - k_2)(v - w)/3, \end{aligned} \quad (22)$$

for cells $j = 0$ or 1 . There are the (dis)continuity conditions which we can apply at $v = w$ or $x = 0$,

$$\begin{aligned} \Psi_1|_{u=r} - \Psi_0|_{u=r} &= 0, \\ (\partial\Psi_1/\partial u)|_{u=r} - (\partial\Psi_0/\partial u)|_{u=r} &= (V/r) \Psi_0|_{u=r}, \end{aligned} \quad (23)$$

as well as the Bloch periodicity conditions,

$$\begin{aligned} \Psi_1|_{u=r} &= e^{2iqr} \cdot \Psi_0|_{u=-r} \\ (\partial\Psi_1/\partial u)|_{u=r} &= e^{2iqr} \cdot (\partial\Psi_0/\partial u)|_{u=-r} \quad , \end{aligned} \quad (24)$$

where q is the (real) quasi-momentum and V corresponds to the size of the δ function barrier. We also remind the reader that the electronic energy is given by $E = (2\hbar^2/3m^2)[k_1^2 + k_2^2 + k_1 k_2]$.

The equations (23) and (24) determine the allowed energy bands from the reality of q via the conditions' combination:

$$(1/2 + \cos(2qr)) [(\alpha + \beta) \cos(\alpha - \beta) - \beta \cos(2\alpha + \beta) - \alpha \cos(\alpha + 2\beta)] + \\ \alpha(\cos \alpha - \cos 2\alpha) + \beta(\cos \beta - \cos 2\beta) - (\alpha + \beta)[\cos(\alpha + \beta) - \cos(2\alpha + 2\beta)] \\ + V[2 \sin \alpha - \sin 2\alpha + 2 \sin \beta - \sin 2\beta - 2 \sin(\alpha + \beta) + \sin(2\alpha + 2\beta)] = 0,$$

where $\alpha \equiv k_1 r, \beta \equiv k_2 r$. With k_1 and k_2 inclined at 120° with respect to one another and $-1 \leq \cos(qr) \leq 1$, one may plot the allowed regions of k_i space for the energy bands. These are drawn in Figures 9 and 10, where we see that if we follow the k_x axis, the bands get narrower as V increases [15]. Indeed as $V \rightarrow \infty$ the ratio $B/A \rightarrow 0$ in equation (22) and the k values become quantized as in the infinite hexagonal well. More generally the energy bands lie between concentric circles at low energies because of the nature of the expression $k_1^2 + k_2^2 + k_3^2$ with triangular axes. For the tight binding model we refer the reader to reference [10].

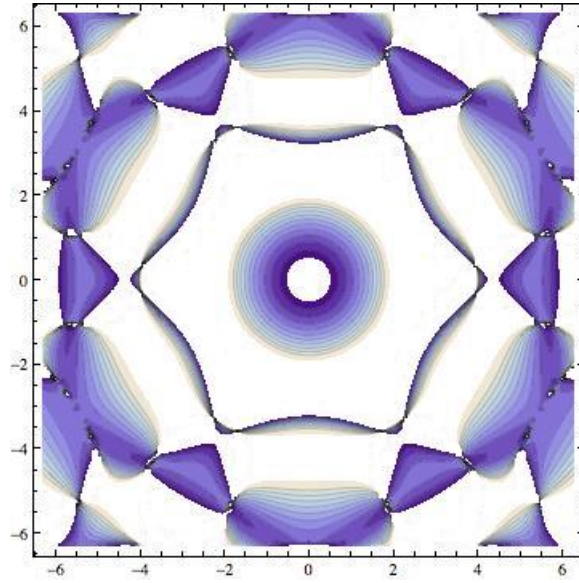


Figure 9: Allowed band (shaded region) for $V = 1$.

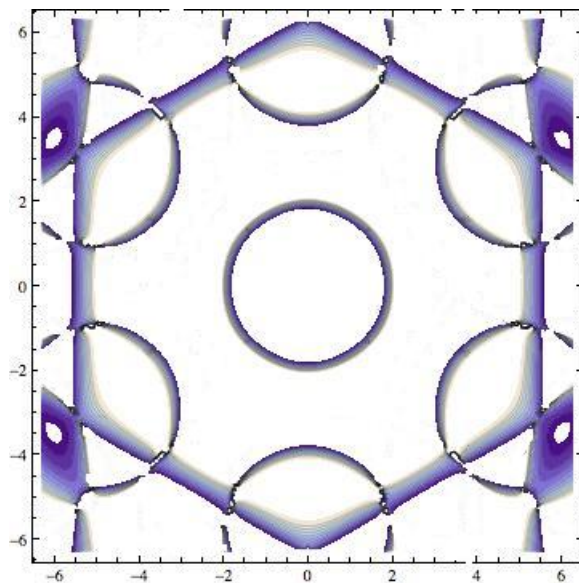


Figure 10: Allowed band (shaded region) for $V = 10$.

6 Conclusions

Our aim in this paper has not been to provide an exhaustive analysis of all properties of graphene, not even in summarized form. Plentiful reviews exist which do just that. Rather our purpose has been to highlight the *symmetry* features to expect from this remarkable material both in the electronic and vibrational characteristics, in the idealized situation that one has an infinite lattice of it. In that way, the directional properties of graphene come much more into evidence. In practice of course we expect the symmetry to be ruined by boundary effects, though the departure is probably significant only near the zigzag and armchair edges.

Graphene is a perfect vehicle for teaching two-dimensional aspects of solid state physics and makes for a very useful variation on the standard theme of square lattices. University teachers can use the material to illustrate many aspects of condensed matter and enlarge the students' horizons.

Acknowledgments

The use of Mathematica has greatly eased the task of producing the various diagrams.

References

- [1] A.K. Geim and K.S. Novoselov, Nature Materials **6**, 183 (2007).
- [2] A.K. Geim and P. Kim, Scientific American, 90, April (2008).
- [3] A.K. Geim, Science **324**, 1530 (2009).
- [4] A.H. Castro-Neto, F. Guinea, N.M.R. Peres, K.S. Novoselov and A.K. Geim, Rev.Mod. Phys. **81**, 109 (2009).
- [5] M.J. Allen, V.C. Tung and R.B. Kaner, Chem. Rev. **110**, 132 (2010).
- [6] J.W. McClure, Phys Rev. **108**, 612 (1957); *ibid* Phys. Rev. **112**, 715 (1958).
- [7] J.C. Charlier, P.C. Eklund, J. Zhu and A.C. Ferrari, Top. Appl. Phys. **111** 673 (2008).
- [8] K.S. Novoselov *et al*, Nature **438**, 197 (2005).
- [9] G. Murguia, A. Raya, A. Sanchez and E. Reyes, Am. J. Phys. **78**,700 (2010).
- [10] P.R. Wallace, Phys. Rev. **71**, 622 (1947).
- [11] A. Matulis and F.M. Peeters, Am. J. Phys. **77**, 595 (2009).
- [12] G. Lamé, J. de l'Ecole Poly. **22**, 194 (1833).
- [13] F. Pockels, "Über die partielle Differentialgleichung $\Delta u + k^2 u = 0$ ", B.G. Teubner, Leipzig (1891).
- [14] B.J. McCartin, Amer. Conf. on Applied Mathematics (MATH '08) Harvard **195**, March (2008), and references therein.
- [15] The result above may be contrasted with the well-known 1D result: $\cos q\ell = \cos k\ell + V (\sin k\ell)/k\ell$.